Accepted Manuscript

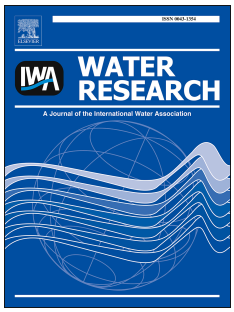

Predicting scale formation during electrodialytic nutrient recovery

Emma Thompson Brewster, Andrew J. Ward, Chirag M. Mehta, Jelena Radjenovic, Damien J. Batstone

PII: S0043-1354(16)30925-3

DOI: 10.1016/j.watres.2016.11.063

Reference: WR 12544

To appear in: *Water Research*

Received Date: 28 September 2016

Revised Date: 28 November 2016

Accepted Date: 28 November 2016

Please cite this article as: Thompson Brewster, E., Ward, A.J., Mehta, C.M., Radjenovic, J., Batstone, D.J., Predicting scale formation during electrodialytic nutrient recovery, *Water Research* (2016), doi: 10.1016/j.watres.2016.11.063.

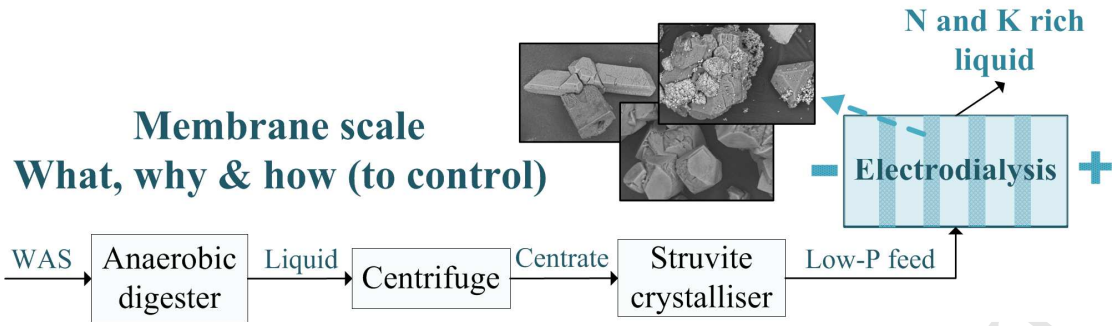

Predicting scale formation during electrodialytic nutrient recovery

Emma Thompson Brewster[1], *Andrew J. Ward*[1], *Chirag M. Mehta*[1], *Jelena Radjenovic*[1,2], *Damien J. Batstone*[1*]

[1]*Advanced Water Management Centre, The University of Queensland, St Lucia, QLD 4072, Australia*

[2]*Catalan Institute for Water Research (ICRA), Parc Científic i Tecnològic de la Universitat de Girona, 17003 Girona, Spain*

Submitted to

Water Research

September 2016

**Corresponding Author:*

Prof. Damien J. Batstone, Advanced Water Management Centre, The University of Queensland, St Lucia, QLD 4072, Australia

Phone: +61 (7) 3346 9051;

Fax: +61 (7) 3365 4726;

Email d.batstone@awmc.uq.edu.au

Abstract

Electro-concentration of nutrients from waste streams is a promising technology to enable resource recovery, but has several operational concerns. One key concern is the formation of inorganic scale on the concentrate side of cation exchange membranes when recovering nutrients from wastewaters containing calcium, magnesium, phosphorous and carbonate, commonly present in anaerobic digester rejection water. Electrodialytic nutrient recovery was trialed on anaerobic anaerobic digester rejection water in a laboratory scale electro-concentration unit without treatment (A), following struvite recovery (B), and following struvite recovery as well as concentrate controlled at pH 5 for scaling control (C). Treatment A resulted in large amount of scale, while treatment B significantly reduced the amount of scale formation with reduction in magnesium phosphates, and treatment C reduced the amount of scale further by limiting the formation of calcium carbonates. Treatment C resulted in an 87±7% by weight reduction in scale compared to treatment A. A mechanistic model for the inorganic processes was validated using a previously published general precipitation model based on saturation index. The model attributed the reduction in struvite scale to the removal of phosphate during the struvite pre-treatment, and the reduction in calcium carbonate scale to pH control resulting in the stripping of carbonate as carbon dioxide gas. This indicates that multiple strategies may be required to control precipitation, and that mechanistic models can assist in developing a combined approach.

Keywords

Electrodialysis; nutrient recovery; membrane scaling; modelling; physico-chemistry; electro-chemistry

Highlights

Struvite pre-precipitation essential for phosphate scaling control

Multiple scale control strategies required for different precipitates

49 Generalized precipitation models effective for the specific case of electrodialysis scaling

50

51 **Nomenclature**

Variable	Meaning
r	Rate of change of concentration of aqueous, gas or solid components (mol m^{-3} s^{-1})
k	Semi-empirical rate coefficient for mineral formation (s^{-1})
S	Aqueous, gas or solid phase species concentration (mol m^{-3})
K_{sp}	Solubility product constant (-)
$k_l a$	The overall film mass transfer coefficient (s^{-1})
K_H	Henry's law constant (mol L^{-1} atm^{-1})
p_{CO2}	Partial pressure of $CO_{2(g)}$ in the atmosphere (atm)
F_{acid}	Flow rate of acid (m^3 s^{-1})
k_{acid}	Proportional control coefficient (-)
pH_{Cres}	pH of the concentrate reservoir (-)

52

53

54

1. INTRODUCTION

Fertilizer price instability due to increasing global demand, energy costs and resource limitations, has put increased pressure on the Australian agriculture industry. It has been identified that a substantial fraction of major macronutrients (100% P and K, 50% N) can be serviced from existing waste streams (Batstone et al. 2015, Mehta et al. 2016). An emerging technology is electro-concentration of ammonium and potassium ions from the waste stream of anaerobic digester supernatant, which has been passed through a centrifuge (hereafter referred to as centrate) (Mehta et al. 2015). Specifically, centrate is a target for nutrient recovery, particularly for ammonium and potassium recovery.

Electrodialysis (ED) is an electrochemical membrane process in which an alternating series of cation exchange membranes (CEMs) and anion exchange membranes (AEMs) are placed between the terminal anode and cathode. Concentrate and diluate solutions are pumped, also in an alternating arrangement, through the chambers between the ion exchange membranes (IEMs). Applying current to the terminal electrodes induced a potential gradient which results in the movement of anions or cations through the AEMs or CEMs, respectively, due to migration. This migration results in the ions becoming concentrated in the concentrate solution.

Membrane processes in water and wastewater treatment, not limited to electro-concentration processes, face the common problem of mineralization of inorganic solids on the surface of the membranes, known as membrane scaling. To address this problem, feed pre-treatment using filtration, coagulation and flocculation or acid addition; use of anti-scalant chemicals; and/or chemical cleaning of the membranes using acidic or basic chemicals is performed, with each treatment option adding cost and operational downtime in the case of membrane

cleaning (Greenlee et al. 2009). More recent studies also suggest the use of *in situ* measures, including application of a pulsed-electric field, as well as electroconvective vortices through operating at overlimiting current to reduce scale formation (Mikhaylin and Bazinet, 2016).

A critical limitation of this application may be the phenomenon of membrane scaling due to concentration polarization, leading to enhanced rates of membrane scale in electrochemical IEM systems being fed with wastewater (Casademont et al. 2007, Xu and Huang 2008, Zhang et al. 2011). Concentration polarization results in higher concentrations of ions on the concentrate side of the CEM and depletion of ions on the diluate side (Baker 2004). Many studies focus on the diluate side concentration polarization phenomenon due the fact that it limits the maximum efficient operating current of the system (Choi et al. 2002, Krol et al. 1999, Kanavova et al. 2014, Nikonenko et al. 2014). In particular, the concentrate side of the membrane is of interest in this study as it is a common site of membrane scaling in many applications where phosphate, calcium, magnesium and/or carbonate are present. The scope of this study considers inorganic membrane scaling across the entire domain of the diluate and concentrate streams. This includes the solution reservoirs, bulk solution in the chambers and the diffusion boundary layers (DBLs) close to the membrane surface. The relatively higher concentrations observed in the solution immediately next to the membrane (as compared to the bulk solution away from the membrane in the chambers and reservoirs) result in a higher saturation index (SI) for certain minerals within this membrane surface boundary layer, compared to the bulk solutions.

While some modelling work has been done to study speciation and acid-base equilibria in electrochemical systems, no models have combined electrochemical and solid-phase physico-chemical mechanisms to study the scaling in ED (Thompson Brewster et al. 2016, Nikonenko

et al. 2003, Dykstra et al. 2014). The aim of this study is to understand the causes and identify control strategies of membrane scaling during ED using centrate feed by developing a dynamic mechanistic model of ED, including precipitation of common scaling minerals. A practical outcome of this study will be to study centrate as a feed (diluate) stream into the ED cell, compared to effluent from an upstream pilot scale struvite crystallizer.

The operation of ED for nutrient recovery from wastewater will differ compared to traditional desalination. It is envisaged that product recovery will be taken from the additional volume accumulating in the concentrate reservoir due to water fluxes from electro-osmosis and osmosis. Operating currents will be 70-90% of the limiting current, and will focus on generating product concentrate with minimal energy input. The model used is capable of approaching limiting current (described mechanistically by depletion of solute ions in the DBLs). Over limiting current mechanisms such as electro-convection are not studied here since above limiting operation is inefficient for ion recovery in this application.

2. METHODS

2.1 Experiments

Reactor configuration

Experiments were performed in a batch-mode, laboratory scale ED unit, with electrolytes, concentrate and diluate being recirculated through reservoirs as shown in Figure 1. The unit was equipped with two CEM membranes (General Electric CR67) and two AEM membranes (General Electric AR204SZRA), each with an effective area of 12 x 14 cm (168 cm^2), and a 20 mm spacing. The amount and thickness of membrane scaling and fouling was not pre-determined and a commonly sized ED cell of 0.3-2 mm spacing would have clogged during even short-term experiments of several hours. Hence wider 20 mm spaces were utilized to

prevent clogging and to enable independent study of the scaling and fouling occurring on each different membrane without cross contamination between different membranes.

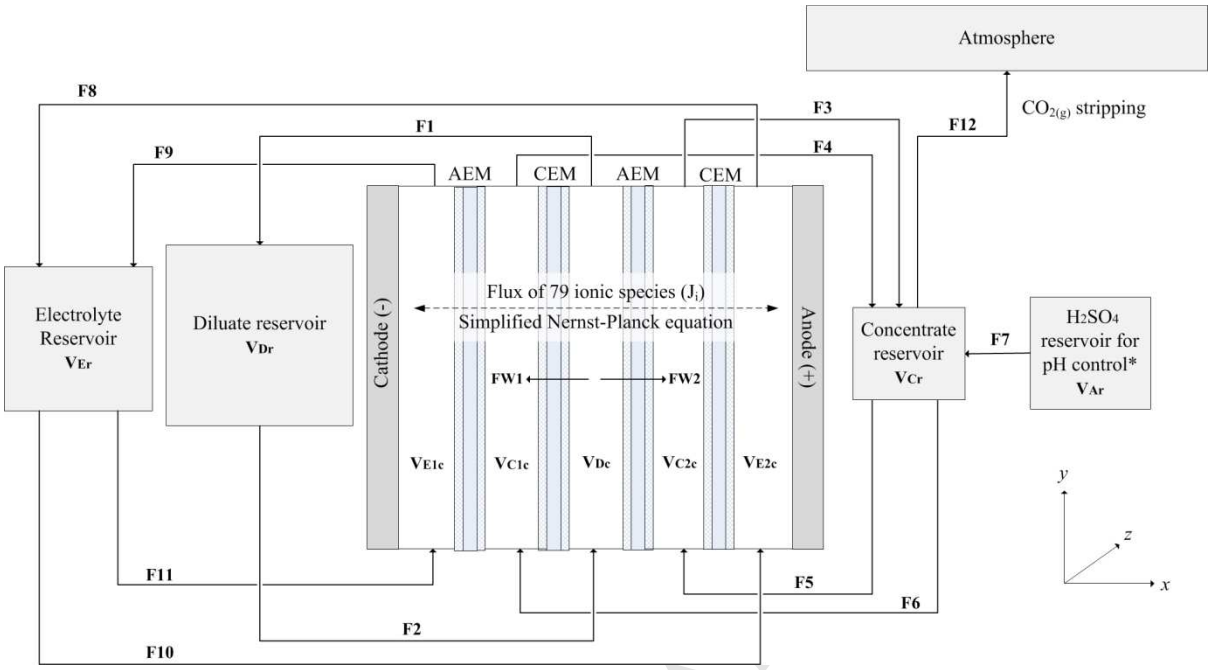

Figure 1: Configuration of the laboratory scale electrodialysis (ED) system. Anion exchange membranes (AEM) and cation exchange membranes (CEM) are shown with diffusion boundary layer (DBL) spatial areas indicated on either side. The scheme shows all modeled streams including convective flows in and out of the reservoirs, water fluxes across the membranes, as well as $CO_{2(g)}$ stripping and acid dosing for pH control in the concentrate reservoir.

A mesh stainless steel cathode and a Ti/$PtIrO_2$ electrode as the anode (Magneto special anodes B V, Netherlands) were utilized. The configuration of the system was anode-CEM-AEM-CEM-AEM-cathode. The reservoirs were vented to maintain atmospheric pressure. A potentiostat (GW INSTEK model GPC 3030) was used to supply a constant current of 500 mA (29.8 A m^{-2}). This current density resulted in formation of scale within the 72 h experimental duration, while also falling within the operational limits of the potentiostat. The

concentrate and diluate streams had a flow rate of 60 mL min^{-1} each. Sodium nitrate (5 g L^{-1}) electrolyte was supplied to the anodic and cathodic compartments at the same flowrate of 60 mL min^{-1} each. Sodium and nitrate ions are highly soluble and should not affect precipitation in the reactor except for their contribution to ionic strength. While cathodic reduction of nitrate is possible, previous work did not observe this to be significant (Thompson Brewster et al. 2016), and it if it did occur it would not significantly impact the key objective of precipitation modelling in the major scale areas in the central chambers of the cell. In full scale application, work should be done to using electrolyte solutions with low propensity for undesirable electrode reactions.

Operating conditions

Three experiments were carried out to evaluate the benefits of two types of anti-scaling treatments compared to using reject wastewater. For the first treatment (treatment A), the initial diluate and concentrate solution was centrate from Luggage Point Sewage Treatment Plant. This is a major wastewater treatment plant (WWTP) in Brisbane, Australia, which treats a mix of domestic and industrial wastewaters. The centrate had been left to settle at minimum overnight with the supernatant decanted for use in the experiments. The first scaling treatment (treatment B) involved passing the centrate solution through a pilot struvite crystallization process also located at Luggage Point WWTP. The struvite crystallization doses sodium hydroxide and magnesium chloride for pH control, and to promote phosphate recovery. The second scaling treatment (treatment C) involved automated H_2SO_4 acid dosing of the concentrate reservoir to maintain a constant pH value of 5, in addition to the struvite crystallization pre-treatment. Initial concentrate and diluate solutions were the same at the start of each experiment. Initial volumes of the diluate, concentrate and electrolyte solutions

were 20, 2 and 10 L for all three treatments, respectively. The electrolyte was replaced as the potential began to reach the limit of the potentiostat (30 V).

Analytical techniques

Sampling was done 7 times during the experimental period, with 30 or 45 mL samples taken from the reservoirs. Elemental analysis was performed using Inductively Coupled Plasma Optical Emission Spectroscopy (ICP-OES) (Perkin Elmer Optima 7300DV, Waltham, MA, USA) after nitric acid digestion for total and soluble cation concentrations (calcium, sodium, potassium, magnesium). Lachat QuickChem8500 Flow Injection Analysis (FIA) (Lachat Instruments, Loveland, CO, USA) was used to measure total soluble NH_4^+-N, PO_4^{3-}-P, NO_x-N and NO_2^--N. The start and finish samples were also analyzed by: ion chromatography (IC) for anions (Dionex ICS-2100 IC system, Dionex, CA, USA); total organic carbon (TOC) and inorganic carbon (TIC) (Shimadzu TOC-L CSH Total Organic Carbon Analyzer with TNM-L TN unit, Kyoto, Japan); gas chromatography for volatile fatty acids (VFA) (Agilent Technologies 7890A GC System, CA, USA); and chemical oxygen demand (COD) (Merck Spectroquant® COD cell tests HC565173 25-1500 mg/L Spectroquant®). Total solids (TS) were measured by evaporating and drying a 10 mL wastewater sample at specified temperature (103 to 105℃). Total suspended solids (TSS) was determined as the difference between TS and total dissolved solid (TDS) as per standard methods (Eaton et al. 1998). Total solution volumes were also measured at the start and end of the experimental period (for the concentrate and diluate) and, before and after electrolyte replacement.

After the experiments, membranes were weighed to evaluate the mass of fouling and scaling accumulated on and within the membrane. As the membranes must remain hydrated before they are used in the experiments, the dry weight was estimated by measuring the percentage

of water weight of clean wet membranes. Three hydrated AEM and CEM samples were cut in 4 cm by 4 cm pieces, patted dry with paper towel and weighed. They were then dried in an oven at 50℃ until they recorded a constant weight, indicating they were completely dry. The percentage of water in a hydrated membrane was then calculated to be 33.7±0.4% and 33.3±0.5% for CEMs and AEMs, respectively. At the completion of the ED experiments, the membranes were dried in the oven under the same conditions as the sample membranes. The final weight was subtracted from the initial weight to estimate the mass of scaling and/or fouling. It is possible some additional scale formed during the drying process. Assuming a worst case scenario of the maximum water loss containing the highest concentrations seen during the experiments, the potential for scale formation would be less or equal to the confidence limits represented in the results.

After the membranes were dried, the composition of the scale was analyzed for bulk characterization using ICP as well as FIA to determine total Kjeldahl nitrogen (TKN) and total phosphorous (TP) (Lachat QuikChem8000 Flow Injection Analyzer, Lachat Instruments, Loveland, CO, USA). Total organic and inorganic carbon in the scale was not possible to quantify as the pH of the solution required to dissolve the minerals would result in stripping of carbon dioxide. Scanning electron microscopy (SEM) (Philips XL30 Scanning Electron Microscope, Philips Electron Optics, Eindhoven, Netherlands) for secondary electron and backscattered electron imaging as well as energy dispersive x-ray analysis (SEM-EDS) (EDAX SiLi detector, AMETEK, USA) was performed to provide further information about the variation in scale size, structure and elemental composition of the scale samples.

2.2 Modelling approach

Physico-electrochemical

The model in this study expanded previous work in Thompson Brewster et al. (2016) to include multi-species ion precipitation and compartment scaling, as well as expansion to a broader range of components, in order to describe real wastewater. The model includes a simplified Nernst-Planck equation to describe mass transport, a charge balance to describe pH, and charge proportioning between multiple counter and co-ions for ion transport through IEMs. Thompson Brewster et al. (2016) integrated the ED model with the speciation model in Flores-Alsina et al. (2015), allowing speciation, ion-pairing and pH effects to be simulated. These methods allow the diffusion and migration of ions to be linked with their speciation relating to pH and ionic strength of the solution in the direction of transport, perpendicular to the electrodes and membranes. The model uses a discretized approach for evaluating the average localized concentrations across different spatial areas in the cell and reservoirs corresponding to Figure 1. Concentrations are dynamically evaluated based on ionic fluxes and water flows between the spatial areas.

For this study, the model in Thompson Brewster et al. (2016) needed to account for real wastewater solutions and expansion of the model from 5 to 11 model components was necessary. The components included total concentrations of sodium, potassium, calcium, magnesium, ammonium, phosphate, nitrate, acetate, chloride, carbonate and sulfate. As a result, this required the expansion of the model to include 79 model species, which include ion pairs as well as species made through acid or base dissociation of the above components (see Table S1.1 for the full list of species). Initial conditions were set to the initial concentrations of the centrate for the concentrate and diluate areas, or, for electrolyte areas, the electrolyte solution described in Section 2.1, or the initial volumes of the variable volume reservoirs as described in Section 2.1. For precipitation states an initial condition of 10^{-11} M

was used. Spatial boundary conditions are zero flux at the electrodes, and zero concentration gradient at the electrodes. It is noted that there are lateral advective flows through concentrate and diluate chambers, but these act on bulk compartments only.

Solid phase chemistry was incorporated to account for the formation of precipitants in all reservoirs, bulk chambers and DBLs in the diluate and concentrate, but excluding the electrolyte. Mbamba et al. (2015) uses a parallel precipitation model using a semi-empirical rate approach, where an independent rate of formation of each of the multiple minerals is calculated from a pool of participating ions. This method was used to calculate the localized formation of mineral precipitants across the different spatial areas of the diluate and concentrate chambers, DBLs and reservoirs. The minerals chosen, based on the criteria in Mbamba et al., (2015), were struvite, amorphous calcium phosphate (ACP), calcium carbonate monohydrate (CCM) and magnesium phosphate. Struvite, ACP and CCM are included as there was evidence to suggest their formation based on the ICP and SEM-EDS results. Struvite, ACP and CCM are known to be common minerals found in wastewater and have been previously modelled in wastewater systems (Mbamba et al. 2015). Magnesium phosphate was added as it was difficult to distinguish the formation of struvite from magnesium phosphate using SEM-EDS due to the low sensitivity to low elemental mass elements like nitrogen (Mikhaylin and Bazinet, 2016). However, only a small amount of magnesium phosphate was obtained from the simulations and model results supported the preferential formation of struvite. Calcium sulfate was not included due to a high K_{SP} = 4.92×10^{-5} (Scott, 2012), and hence calcium sulfate never had a SI>1 in any part of the domain.

Chemical precipitation formation equations are shown in Equations 1 to 4, for struvite, ACP, CCM and magnesium phosphate, respectively, where *r* is the rate of formation or dissolution (mol m^{-3} s^{-1}), *k* is the semi-empirical rate coefficient (s^{-1}), and *S* is the state variable concentration of the species (mol m^{-3} for mineral species, mol L^{-1} for aqueous species). Scale formation only occurred if the SI of the mineral was greater than one; if the SI was less than one, mineral dissolution occurred. Rates of dissolution were modelled empirically using the same equation as formation, with the final exponent term decreased to 1 to account for the diffusion limitation of dissolution reactions (Mbamba et al. 2015). During these studies precipitation was the dominant mechanism. The semi-empirical rate coefficients and the pKsp values used in the model were 5, 0.5, 5 and 1 h^{-1} and 13.26, 7.144, 25.46 and 23.98 for struvite, CCM, ACP and magnesium phosphate, respectively (Scott, 2012, Mbamba et al. 2015).

$$r_{stru} = k_{stru} S_{stru} \left(\left(\frac{S_{NH4} S_{Mg} S_{PO4}}{K_{sp,stru}} \right)^{1/3} - 1 \right)^3 \quad (1)$$

$$r_{ACP} = k_{ACP} S_{ACP} \left(\left(\frac{S_{Ca}{}^3 S_{PO4}{}^2}{K_{sp,ACP}} \right)^{1/5} - 1 \right)^2 \quad (2)$$

$$r_{CCM} = k_{CCM} S_{CCM} \left(\left(\frac{S_{Ca} S_{CO3}}{K_{sp,CCM}} \right)^{1/2} - 1 \right)^2 \quad (3)$$

$$r_{MgP} = k_{MgP} S_{MgP} \left(\left(\frac{S_{Mg}{}^3 S_{PO4}{}^2}{K_{sp,MgP}} \right)^{1/5} - 1 \right)^2 \quad (4)$$

Mbamba et al. (2015) developed this model in three parts: equilibrium, kinetic and gas transfer. The equilibrium set of algebraic equations is similar to the one used here to account

for the speciation and acid-base pairings. The kinetic part is included by adding to and amending the set of ODEs used to describe the concentrations of ions in the ED cell by adding one state equation for each precipitant in each spatial area for the diluate and concentrate parts of the cell and reservoirs. A limitation of the precipitation model is that precipitation of solids inside the membrane itself will not occur, as the membrane is not considered a spatial domain in the finite element matrix.

Gas transfer of CO_2 was included as shown in Equation 5, where r is the rate of $CO_{2(g)}$ formation (mol m^{-3} s^{-1}), $k_l a$ is the overall film mass transfer coefficient (0.001 s^{-1}), $S_{CO2(aq)}$ is the concentration of dissolved carbon dioxide in the liquid bulk phase as calculated in the equilibrium part of the model (mol L^{-1}), K_H is the Henry's law constant (0.034 mol L^{-1} atm^{-1}) and $p_{CO2(g)}$ is the partial pressure of $CO_{2(g)}$ (0.00032 atm) (Mbamba et al. 2015). $NH_{3(g)}$ stripping was not included as it was not observed to occur during the experiments.

$$r_{CO_{2(g)}} = k_l a\left(S_{CO_{2(aq)}} - K_H\, p_{CO_{2(g)}}\right)\times 1000 \qquad (5)$$

Water transport

The experiments showed significant increases (175% to 335%) in concentrate reservoir volume over the course of the experiments (see Table S4.1) due to the water transport caused by osmosis and electro-osmosis (Pronk et al. 2006). To account for the impact of water flux on the concentrate concentrations, the state equations for the diluate and concentrate reservoirs and chambers were expanded by removing the constant volume assumptions in the reservoirs and including an additional water flux term into the diluate and concentrate

chambers. The state equations used in the model corresponding to nomenclature in Figure 1 are shown in Equations S2.1-S2.43.

Concentrate pH control

To simulate treatment C, the model included acid dosing to maintain the concentrate pH at pH 5 by using a proportional control loop. This control loop added a flow of sulfuric acid in order to match the calculated pH in the concentrate reservoir (pH_{Cres}) to the set point pH (5) using Equation 6, where F_{acid} is the flow rate of acid (m^3 s^{-1}) and k_{acid} is the proportional control coefficient (10^{-7}).

$$F_{acid} = k_{acid}\left(pH_{C_{res}} - 5\right) \quad (6)$$

3. RESULTS AND DISCUSSION

3.1 Wastewater characterization

Anaerobic digester centrate was collected from Luggage Point WWTP, Brisbane, during February and March 2016. The pH, TSS, COD, total and soluble Ca, total and soluble Mg, soluble PO_4^{3-}-P and soluble NH_4^+-N of the centrate used in this study were compared against longer tern data (January-April 2016) (Table S3.1, Figure S3.1). The comparison indicates that for most of the parameters the experimental wastewater has similar composition to the average values taken during the almost four months of baseline comparison data. On average, over the baseline comparison period the struvite crystallization process removed 86±8% and 27±8% of the phosphorous and calcium, respectively, while it increased the magnesium concentration due to addition of magnesium chloride by 292±271% (an average concentration increase of 1.82 mM) compared to the average value for direct centrate. During this time, a separate study on magnesium dosing was being carried out at the struvite pilot

plant, which contributed to the high variability in the magnesium concentrations. In treatment C the influent total and soluble Mg were over 20 times higher than for the other two treatments. This is likely due to reduced phosphate concentration in the centrate, leading to a temporary overdose of Mg in the struvite crystallizer just prior to the collection period.

3.2 Experimental results

Membrane fouling and scaling

Formation of a white scale was observed on the concentrate side of the inner CEM (Cc) for treatment A and B (Figures S5.2 and S5.6). A layer of brown fouling was formed on the diluate side of the inner AEM (Aa) in all treatments (Figures S5.3, S5.7 and S5.11). Figure 2 shows the masses of membrane fouling and scaling observed on each membrane during the three consecutive runs. Using upstream struvite precipitation reduced the majority of scaling for the inner CEM membrane, i.e. the CEM closest to the cathode (Cc), and controlling the pH at pH 5 reduced it further. Using combined pre-treatment and pH control (treatment C) reduced the amount of scaling on this CEM by 87±7% compared to the direct centrate (treatment A). Furthermore, pH control of the concentrate did not make a difference to membrane fouling on the inner AEM, i.e. the AEM closest to the anode (Aa). However, using struvite crystallization pre-treatment significantly reduced the amount of membrane fouling on the inner AEM during both treatments B and C by 64±8% and 63±10%, respectively. While modelling organic fouling is not within the scope of this study, this is a reasonable topic for future analysis, including the effect of struvite pre-treatment on organic fouling reduction. Organic foulants could be included in the model as partially charged complex organics which precipitate above a specific threshold (considering also the charge change

with pH). There is, however, a substantial amount of fundamental research needed to support this model.

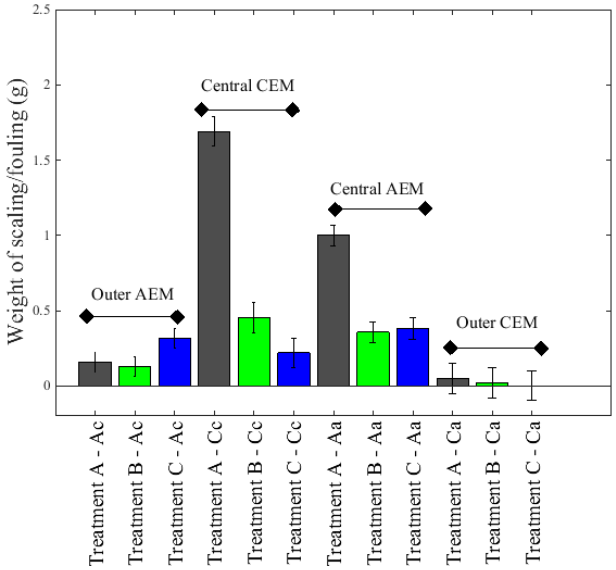

Figure 2: Mass of membrane fouling and scaling where Ac and Cc represent anion and cation exchange membranes closest to the cathode, respectively. Aa and Ca represent anion and cation exchange membranes closest to the anode, respectively. Treatments A, B and C are shown in dark grey (darkest), green (lightest) and blue, respectively.

After drying the membranes, any recoverable scale was analyzed using ICP, TKN, TP as well as SEM-OES. Table 1 shows the results of the bulk characterization of the scale using ICP, TKN and TP on all parts of the experimental membranes where it was observed to occur. The cation components in the scale include calcium, magnesium and nitrogen. Phosphorous is the only anion which was analyzed in the scale, but it is likely that carbonate precipitants are also present based on aqueous phase concentrations of TIC. A summary of the SEM-OES observations about scale size, composition and shape for the 6 scale samples is also in Table 1. SEM-OES images and frequency graphs are in Figures S6.1 to S6.75.

374 Table 1: Summary of the composition of scale formed during the three ED experiments.

Sample	**Ca (ICP) (mM/g)**	**Mg (ICP) (mM/g)**	**P (TP) (mM/g)**	**TKN (TKN) (mM/g)**	**SEM-OES summary** **(Note: nitrogen is difficult to detect using this method)**
Treatment A inner CEM (Cc) concentrate side	3.50	2.79	2.99	1.82	Varied composition, size and structure. Indicated elemental combinations include calcium, carbon and oxygen; magnesium, phosphorous and oxygen; and calcium, phosphorous and oxygen.
Treatment A inner AEM (Aa) concentrate side	3.87	1.72	3.91	1.52	Varied composition, size and structure. Indicated elemental combinations include calcium, phosphorous and oxygen; and magnesium, phosphorous and oxygen.
Treatment B inner CEM (Cc) concentrate side	8.12	0.13	0.10	0.07	Consistent, small shape and composition. The only indicated elemental combination includes calcium, carbon and oxygen.
Treatment B inner AEM (Aa) concentrate side	0.25	4.28	N/A	N/A	Some variation in shape, size and composition. Indicated elemental combinations include calcium, carbon and oxygen; and magnesium, phosphorous and oxygen. Organics present.
Treatment C inner AEM (Aa) concentrate side	0.03	4.75	4.10	2.11	Consistent large size and composition. Indicated elemental combinations include either low or high carbon content magnesium, phosphorous and oxygen
Treatment C outer AEM (Ac) concentrate side	0.02	3.56	3.24	2.03	Consistent large size and composition. Indicated elemental combinations include either low or high carbon content magnesium, phosphorous and oxygen

375

3.3 Modelling results

Model calibration for the $CO_{2(g)}$ k_la value and effective membrane resistance fraction was conducted using the data from treatment A, and validated using the data from treatments B and C. The full experimental and modelled results are shown in Figure S7.1, and have been summarized into a normalized correlation scatter plot in Figure 3, which has an associated normalized R^2 value of 0.77. Further discussion of the calibration may be found in Section 3.5.

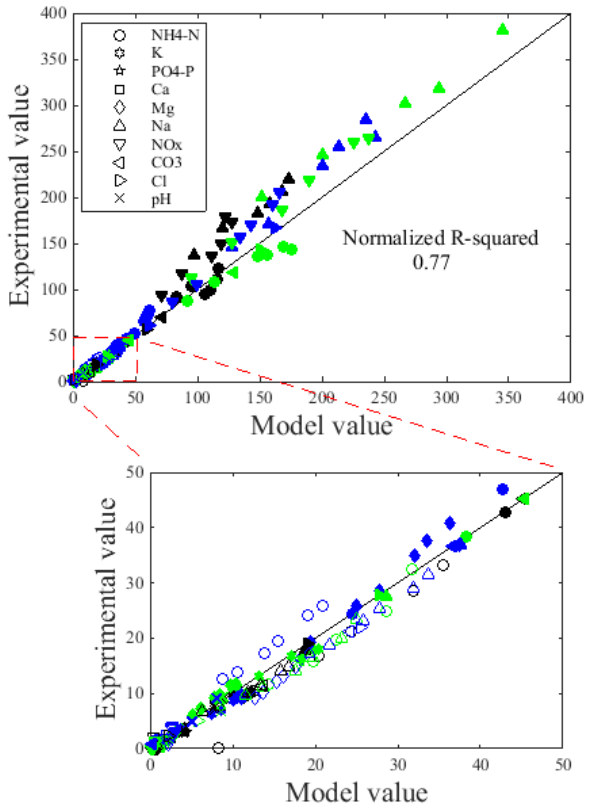

Figure 3: Normalized correlation plot comparing the model components and pH to treatments A, B and C shown here in black (darkest), green (lightest) and blue, respectively.

Figure 4 shows the model output for the concentration of each precipitant across all spatial areas of the diluate and concentrate chambers and DBLs of the ED cell. The notably higher

389 concentrations in the concentrate DBLs next to the inner membranes indicate that the model
390 is consistent with the experimental observations of where the mineralization occurred. In
391 addition, the model is consistent with the observations of the types of mineralizing elements
392 described in Table 1. While conditions leading to supersaturation were expected on both the
393 inner CEM and AEM concentrate sides during treatment A and B. The pH control of the
394 concentrate in treatment C was ineffective to sufficiently lower the SI of struvite and prevent
395 scale formation in this area.

396

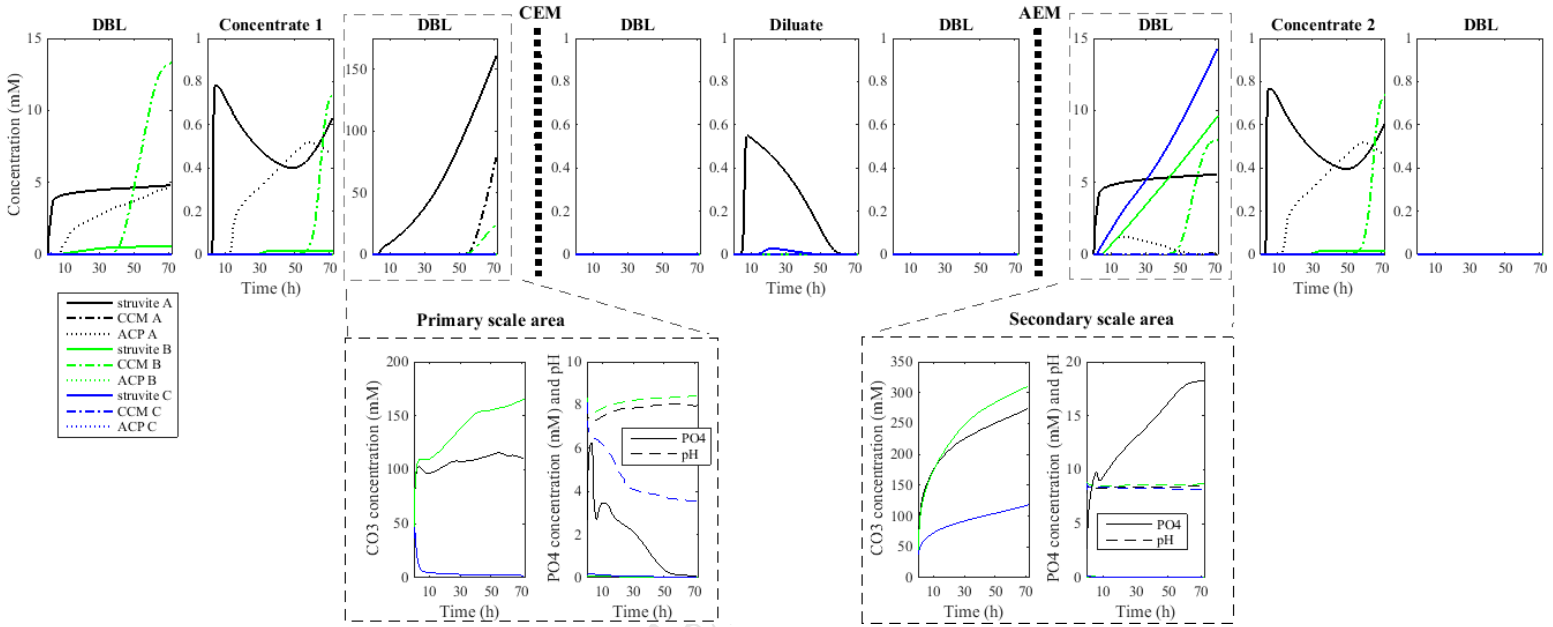

397

398 Figure 4: Modelled precipitation in the diluate and concentrate chambers and diffusion boundary layers (DBLs) for each of the three
399 electrodialysis (ED) treatments. From left to right shows the DBLs and chambers of the cell, with the orientation of the cathode to the left and
400 the anode to the right; the location of the inner cation exchange membrane (CEM) and anion exchange membrane (AEM) are shown for
401 references to their location in the cell. Treatments A, B and C are shown in black (darkest), green (lightest) and blue, respectively.

3.4 Mechanisms contributing to membrane scaling

Figure 4 shows the simulated results occuring in the DBL spatial area at the major scaling site on the concentrate side of the central CEM for the three treatments. The inlays in Figure 4 show that the struvite pre-treatment in treatments B and C depleted the initial concentrations of phosphorous such that formation of struvite was limited. This explaination based on PO_4^{3-} limitation is supported by similar NH_4^+ concentrations, Mg^{2+} concentrations and pH in treatment B compared to treatment A. In treatment C, the pH of the concentrate stream was controlled at pH 5, resulting in the speciation of carbonate to be driven towards $H_2CO_{3(aq)}$ instead of $CO_{3(aq)}^{2-}$ and $HCO_{3(aq)}^-$ (noting that mathematically $H_2CO_{3(aq)}$ is equivalent to $CO_{2(aq)}$). The rate of $CO_{2(g)}$ stripping is driven by the concentrations of $H_2CO_{3(aq)}$ ($CO_{2(aq)}$), which in the case of pH controlled at pH 5 is much higher. Therefore, more carbonate leaves the system as gas resulting in the depletion of the aqueous carbonate component as seen in the inlays of Figure 4. This depletion of carbonate results in a SI below 1 for CCM and less precipitation occurring. The acid-base dissociation framework used in the model is generally applicable to any solution that contains these components. However, this study has highlighted the physico-chemically described speciation of carbonate as a key aspect of scale formation. Generalized speciation models could be a useful took to evaluate scale formation, particularly during overlimiting current applications such as Cifuentes-Araya et al. (2013) and Mikhaylin et al. (2016), where steep ionic concentration gradients may exist.

3.5 Calibration analysis

Compared to the original membrane transport model described in Thompson Brewster et al. (2016), the modelled effective membrane resistance to ion transport was increased an order of magnitude in order to fit the concentration profiles over time. This includes protons and

hydroxide ions as they function as co-ions. Since migration is fixed by the overall current, the main effective change is balance between ionic back diffusion versus forward migration. It is likely that the Membranes International Inc. membranes (Membranes International Inc., 2016a, 2016b) used in Thompson Brewster et al. (2016) have electrical resistances which differ to the membranes used here. Due to different test conditions used to evaluate manufacturer membrane resistances these values are difficult to compare without the use of a standardized model (such as used here). This model parameter (the effective membrane resistance to ion transport) appears to be very important, particularly for electrodialytic nutrient recovery, as it affects the back diffusion of ions and the maximum concentrations in the concentrate stream. These are both key issues to the practical application of electrodialytic nutrient recovery, and the balance of membrane selectivity versus resistance for mixed ions has not been covered extensively in the literature. This additional effective membrane resistance benefits the increase in concentration would need to be practically evaluated in regards to the resulting increase in energy consumption, but such a study is beyond the scope of this paper.

3.6 Implications for design and application

This study demonstrated that scaling in ED with real wastewater occurs due to inorganic species such as PO_4^{3-}, NH_4^{+}, Mg^{2+}, Ca^{2+} and CO_3^{2-}, which form low-solubility minerals. The formation of struvite scale can by limited by removal of phosphate from the aqueous phase, while in the case of calcium carbonates it is aqueous carbon dioxide that needs to be removed. The intended use of this technology is downstream of a struvite recovery unit for reject centrate liquor in a standard WWTP. The main outcome of this study is that coupling these technologies is useful for scale control during ED with wastewater relatively high in phosphorous. The more effective the struvite recovery unit is at removing all the phosphate,

452 and if possible calcium, from the wastewater, the less scale will be formed and therefore the
453 maintenance costs for the ED unit will be lower. However, due to its main purpose, the
454 struvite recovery unit does not reduce the calcium or carbonate concentrations as much as the
455 phosphorous. It is noted that pH control of the concentrate is far more expensive (due to
456 chemical consumption) than phosphate removal, and hence there is a hierarchy of control
457 measures. Use of aeration pre-treatment for struvite crystallization to raise the pH may be
458 beneficial as it is known to remove carbonates in addition to promoting struvite formation.
459 Based on the mass of scale formed during the different treatments, it is estimated that the *in*
460 *situ* scale reduction treatment C would extend the need for a shut-down chemical cleaning
461 using acid-wash by approximately 7 times compared to treatment A. While this study used
462 spacers of 20 mm, spacers of 5-10 mm are envisaged for pilot and full scale operation using
463 centrate feed based on the scale control treatments identified here.
464
465 The description of scale prevention here is very similar to Shaffer and Mintz (1966), their key
466 recommendation is to keep the solution below the supersaturation limit. The model developed
467 here can be used to dynamically identify which conditions will lead to the supersaturation
468 limit in the complex solutions and in spatial areas where it is difficult to pre-determine the
469 concentrations, for example in DBLs. This coupled electrochemical and physico-chemical
470 modelling tool should be used for processes where scaling is likely to occur, such as dairy
471 processing (Casademont et al. 2007, Casademont et al. 2008), phosphate recovery from
472 reverse osmosis concentrate (Zhang et al. 2013), or other applications concerning nutrient
473 recovery from faeces or urine streams (Ledezma et al. 2015, Mondor et al. 2009). This study
474 highlights the usefulness of ED as a nutrient recovery technology for domestic centrate
475 wastewater which is low in phosphate. However, due to the complex physico-chemistry of
476 electrochemical technologies, we hesistate to nominate ED as a optimal technology of any

liquid stream low in phosphate, as calcium and magnesium based scales are common occurances in many systems. Model based analysis using the specific concentrate and diluate conditions would be necessary to perform before coming to such a conclusion for other types of wastewater.

Future studies could study scale control using pulsed-modes of current, membranes with different properties and electroconvective vortices which occur at overlimiting current (Cifuentes-Araya et al. 2013, Cifuentes-Araya et al. 2014, Mikhaylin et al., 2014, Mikhaylin & Bazinet, 2016). In addition, prior to full-scale operation, organic fouling formed on the diluate side of the AEM should be analyzed to determine whether pre-treatment removal or ED reversal (EDR) need to be applied to control fouling formation.

4. CONCLUSIONS

The combination of struvite removal pre-treatment and pH control at pH 5 reduced the amount of mineral scale observed during electro-concentration of real domestic reject wastewater. There is also preliminary evidence to suggest struvite pre-treatment reduced the amount of organic fouling in the system. A mechanistic model describing the behaviour of inorganic ions including aqueous, solid and gas phase physico-chemistry was developed. The model indicated that the mechanisms behind scale control on the concentrate side of the CEM were the removal of a limiting struvite component (phosphate) through the struvite crystallization pre-treatment and stripping of the carbonate component as $CO_{2(g)}$ which prevented the formation of CCM.

ACKNOWLEDGEMENTS

This research was supported financially by the Grain Research & Development Corporation (GRDC) under the project UQ00061: Fertilizer from Waste Phase II as well as through a Grain Research Scholarship (GRS10661) supporting Emma Thompson Brewster. The authors acknowledge the facilities, and the scientific and technical assistance, of the Australian Microscopy & Microanalysis Research Facility at the Centre for Microscopy and Microanalysis, The University of Queensland. The authors also thank the facilities, and the scientific and technical assistance of the Analytical Services Laboratory at the Advanced Water Management Centre, The University of Queensland. Queensland Urban Utilities (QUU) is acknowledged for their supply of wastewater and collaboration in building the Innovation Centre which houses the pilot struvite crystallizer. Dr. Christian K. Mbamba, Dr. Stephan Tait and Dr. Xavier Flores-Alsina are also thanked for their assistance regarding physico-chemical modelling.

REFERENCES

Baker, R.W. (2004) Membrane Technology and Applications, pp. 161-190, John Wiley & Sons, Ltd.

Batstone, D.J., Hulsen, T., Mehta, C.M. and Keller, J. (2015) Platforms for energy and nutrient recovery from domestic wastewater: A review. Chemosphere 140, 2-11.

Casademont, C., Farias, M.A., Pourcelly, G. and Bazinet, L. (2008) Impact of electrodialytic parameters on cation migration kinetics and fouling nature of ion-exchange membranes during treatment of solutions with different magnesium/calcium ratios. Journal of Membrane Science 325(2), 570-579.

Casademont, C., Pourcelly, G. and Bazinet, L. (2007) Effect of magnesium/calcium ratio in solutions subjected to electrodialysis: Characterization of cation-exchange membrane fouling. Journal of Colloid and Interface Science 315(2), 544-554.

Choi, J.H., Park, J.S. and Moon, S.H. (2002) Direct measurement of concentration distribution within the boundary layer of an ion-exchange membrane. Journal of Colloid and Interface Science 251(2), 311-317.

Cifuentes-Araya, N., Pourcelly, G. and Bazinet L. (2013) Water splitting proton-barriers for mineral membrane fouling control and their optimization by accurate pulsed modes of electrodialysis. Journal of Membrane Science 447, 433-441.

Cifuentes-Araya, N., Astudillo-Castro, C. and Bazinet, L. (2014) Mechanisms of mineral membrane fouling growth modulated by pulsed modes of current during electrodialysis: Evidences of water splitting implications in the appearance of the amorphous phases of magnesium hydroxide and calcium. Journal of Colloids and Interface Science 426, 221-234.

536 Dykstra, J.E., Biesheuvel, P.M., Bruning, H. and Ter Heijne, A. (2014) Theory of ion
537 transport with fast acid-base equilibrations in bioelectrochemical systems. Physical Review E
538 90(1).
539 Eaton, A.D., Clesceri, L.S., Greenberg, A.E. and Franson, M.A.H. (1998) Standard methods
540 for the examination of water and wastewater, American Public Health Association,
541 Washington, DC.
542 Ekama, G.A., Wentzel, M.C. and Loewenthal, R.E. (2006) Integrated chemical-physical
543 processes kinetic modelling of multiple mineral precipitation problems. Water Science and
544 Technology 53(12), 65-73.
545 Flores-Alsina, X., Mbamba, C.K., Solon, K., Vrecko, D., Tait, S., Batstone, D.J., Jeppsson,
546 U. and Gernaey, K.V. (2015) A plant-wide aqueous phase chemistry module describing pH
547 variations and ion speciation/pairing in wastewater treatment process models. Water
548 Research 85, 255-265.
549 Greenlee, L.F., Lawler, D.F., Freeman, B.D., Marrot, B. and Moulin, P. (2009) Reverse
550 osmosis desalination: Water sources, technology, and today's challenges. Water Research
551 43(9), 2317-2348.
552 Kanavova, N., Machuca, L. and Tvrznik, D. (2014) Determination of limiting current density
553 for different electrodialysis modules. Chemical Papers 68(3), 324-329.
554 Krol, J.J., Wessling, M. and Strathmann, H. (1999) Concentration polarization with
555 monopolar ion exchange membranes: current-voltage curves and water dissociation. Journal
556 of Membrane Science 162(1-2), 145-154.
557 Ledezma, P., Kuntke, P., Buisman, C.J.N., Keller, J. and Freguia, S. (2015) Source-separated
558 urine opens golden opportunities for microbial electrochemical technologies. Trends in
559 Biotechnology 33(4), 214-220.
560 Mbamba, C.K., Tait, S., Flores-Alsina, X. and Batstone, D.J. (2015) A systematic study of
561 multiple minerals precipitation modelling in wastewater treatment. Water Research 85, 359-
562 370.
563 Mehta, C., Tucker, R., Poad, G., Davis, R., McGahan, E., Galloway, J., O'Keefe, M., Trigger,
564 R. and Batstone, D. (2016) Nutrients in Australian agro-industrial residues: Production,
565 characteristics and mapping. Australasian Journal of Environmental Management 23(2), 206-
566 222.
567 Mehta, C.M., Khunjar, W.O., Nguyen, V., Tait, S. and Batstone, D.J. (2015) Technologies to
568 recover nutrients from waste streams: A critical review. Critical Reviews in Environmental
569 Science and Technology 45(4), 385-427.
570 Membranes International Inc. (2016a) CMI-7000 cation exchange membranes technical
571 specifications, viewed 27/9/2016 at http://www.membranesinternational.com/tech-cmi.htm.
572 Membranes International Inc. (2016b) AMI-7001 anion exchange membrane technical
573 specifications, viewed 27/9/2016 at http://www.membranesinternational.com/tech-ami.htm.
574 Mikhaylin, S., Nikonenko, V., Pourcelly. G. and Bazinet, L. (2014) Intensification of
575 demineralization process and decrease in scaling by application of pulsed electric field with
576 short pulse/pause conditions. Journal of membrane Science 468, 389-399;
577 Mikhaylin, S. and Bazinet, L. (2016) Fouling on ion-exchange membranes: Classification,
578 characterization and strategies of prevention and control. Advances in Colloid and Interface
579 Science 229, 34-56.
580 Mikhaylin, S., Nikonenko, V., Pismenskaya, **N.,** Pourcelly, G., Choi S., Kwon H.J., Han, J.,
581 Bazinet, L., (2016) How physico-chemical and surface properties of cation-exchange
582 membrane affect membrane scaling and electroconvective vortices: influence on performance
583 of electrodialysis with pulsed electric field. Desalination 393, 102-114.

584 Mondor, M., Ippersiel, D., Lamarche, F. and Masse, L. (2009) Fouling characterization of
585 electrodialysis membranes used for the recovery and concentration of ammonia from swine
586 manure. Bioresource Technology 100(2), 566-571.
587 Nikonenko, V., Lebedev, K., Manzanares, J.A. and Pourcelly, G. (2003) Modelling the
588 transport of carbonic acid anions through anion-exchange membranes. Electrochimica Acta
589 48(24), 3639-3650.
590 Nikonenko, V.V., Kovalenko, A.V., Urtenov, M.K., Pismenskaya, N.D., Han, J., Sistat, P.
591 and Pourcelly, G. (2014) Desalination at overlimiting currents: State-of-the-art and
592 perspectives. Desalination 342, 85-106.
593 Pronk, W., Biebow, M. and Boller, M. (2006) Electrodialysis for recovering salts from a
594 urine solution containing micropollutants. Environmental Science & Technology 40(7),
595 2414-2420.
596 Scott, J. (2012) CRC handbook of chemistry and physics: Student edition, Access
597 Intelligence, LLC., Boca Raton, Fla.
598 Shaffer, L.H. and Mintz, M.S. (1966) Principles of Desalination. Spiegler, K.S. (ed),
599 Academic Press.
600 Thompson Brewster, E., Mehta, C.M., Radjenovic, J. and Batstone, D.J. (2016) A
601 mechanistic model for electrochemical nutrient recovery systems. Water Research 94, 176-
602 186.
603 Xu, T.W. and Huang, C.H. (2008) Electrodialysis-Based Separation Technologies: A Critical
604 Review. Aiche Journal 54(12), 3147-3159.
605 Zhang, Y., Desmidt, E., Van Looveren, A., Pinoy, L., Meesschaert, B. and Van der Bruggen,
606 B. (2013) Phosphate Separation and Recovery from Wastewater by Novel Electrodialysis.
607 Environmental Science & Technology 47(11), 5888-5895.
608 Zhang, Y., Ghyselbrecht, K., Meesschaert, B., Pinoy, L. and Van der Bruggen, B. (2011)
609 Electrodialysis on RO concentrate to improve water recovery in wastewater reclamation.
610 Journal of Membrane Science 378(1–2), 101-110.

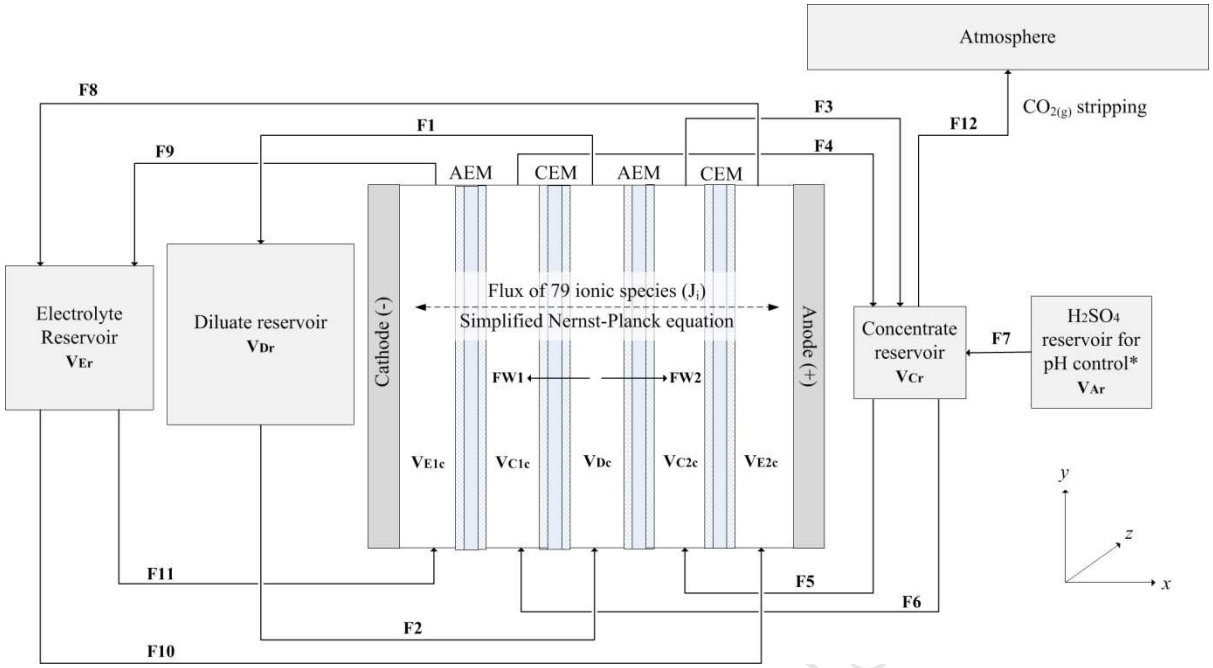

Figure 1: Configuration of the laboratory scale electrodialysis (ED) system. Anion exchange membranes (AEMs) and cation exchange membranes (CEMs) are shown with diffusion boundary layer (DBL) spatial areas indicated on either side. The scheme shows all modeled streams including convective flows in and out of the reservoirs, water fluxes across the membranes, as well as $CO_{2(g)}$ stripping and acid dosing for pH control in the concentrate reservoir.

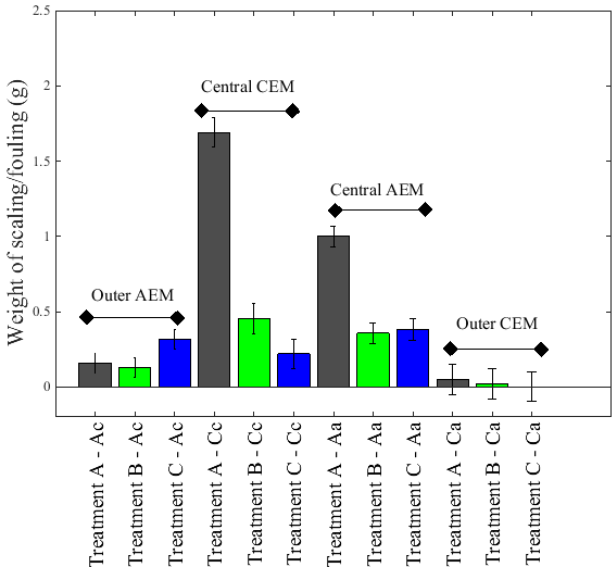

Figure 2: Mass of membrane fouling and scaling where Ac and Cc represent anion and cation exchange membranes closest to the cathode, respectively. Aa and Ca represent anion and cation exchange membranes closest to the anode, respectively. Treatments A, B and C are shown in dark grey (darkest), green (lightest) and blue, respectively.

15

16 Table 1: Summary of the composition of scale formed during the three ED experiments.

Sample	**Ca (ICP) (mM/g)**	**Mg (ICP) (mM/g)**	**P (TP) (mM/g)**	**TKN (TKN) (mM/g)**	**SEM-OES summary** **(Note: nitrogen is difficult to detect using this method)**
Treatment A inner CEM (Cc) concentrate side	3.50	2.79	2.99	1.82	Varied composition, size and structure. Indicated elemental combinations include calcium, carbon and oxygen; magnesium, phosphorous and oxygen; and calcium, phosphorous and oxygen.
Treatment A inner AEM (Aa) concentrate side	3.87	1.72	3.91	1.52	Varied composition, size and structure. Indicated elemental combinations include calcium, phosphorous and oxygen; and magnesium, phosphorous and oxygen.
Treatment B inner CEM (Cc) concentrate side	8.12	0.13	0.10	0.07	Consistent, small shape and composition. The only indicated elemental combination includes calcium, carbon and oxygen.
Treatment B inner AEM (Aa) concentrate side	0.25	4.28	N/A	N/A	Some variation in shape, size and composition. Indicated elemental combinations include calcium, carbon and oxygen; and magnesium, phosphorous and oxygen. Organics present.
Treatment C inner AEM (Aa) concentrate side	0.03	4.75	4.10	2.11	Consistent large size and composition. Indicated elemental combinations include either low or high carbon content magnesium, phosphorous and oxygen
Treatment C outer AEM (Ac) concentrate side	0.02	3.56	3.24	2.03	Consistent large size and composition. Indicated elemental combinations include either low or high carbon content magnesium, phosphorous and oxygen

17

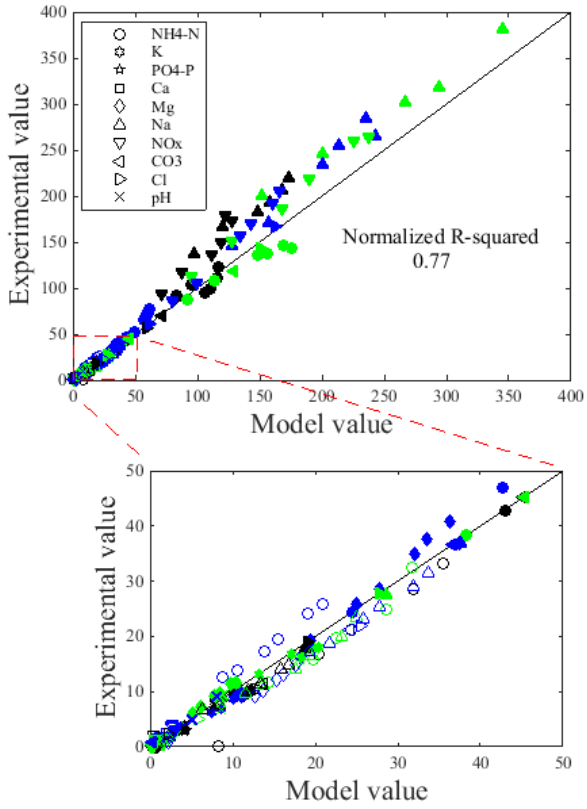

18

19 Figure 3: Normalized correlation plot comparing the model components and pH to treatments

20 A, B and C shown here in black (darkest), green (lightest) and blue, respectively.

21

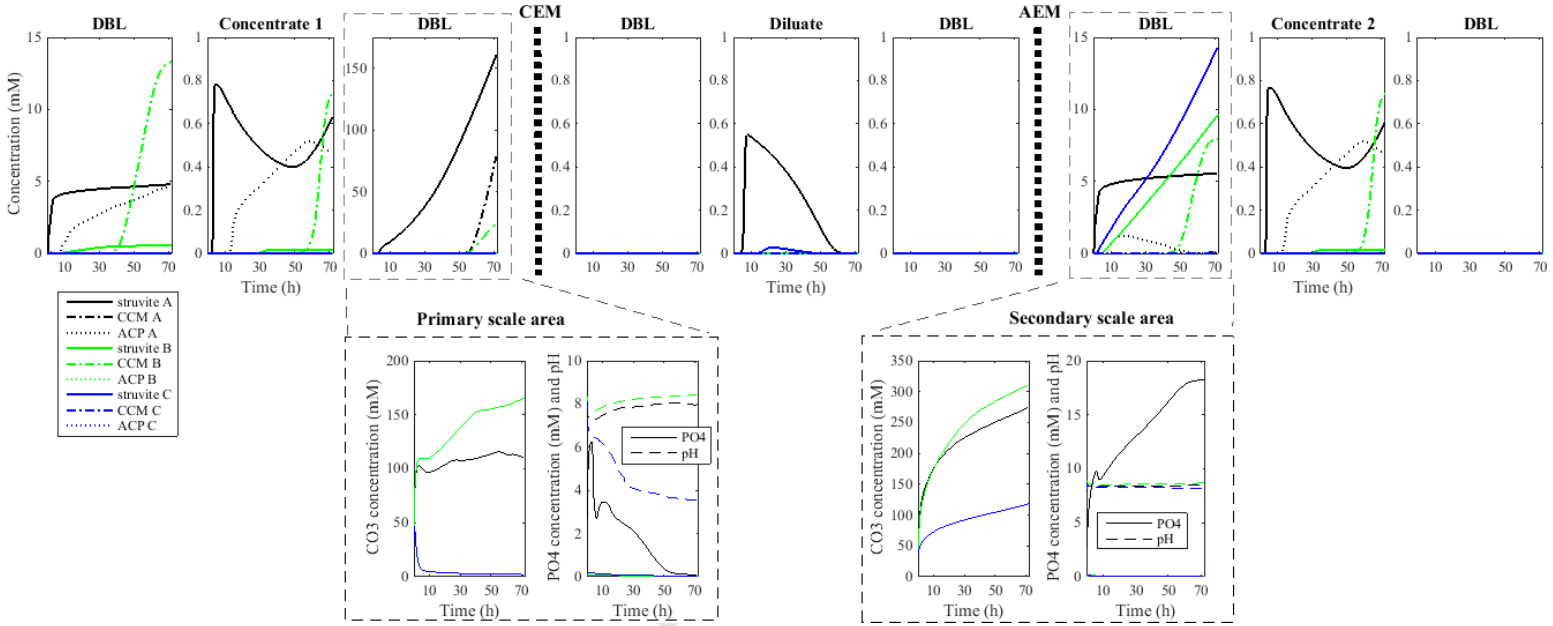

Figure 4: Modelled precipitation in the diluate and concentrate chambers and diffusion boundary layers (DBLs) for each of the three electrodialysis (ED) treatments. From left to right shows the DBLs and chambers of the cell, with the orientation of the cathode to the left and the anode to the right; the location of the inner cation exchange membrane (CEM) and anion exchange membrane (AEM) are shown for reference to their locations in the cell. Treatments A, B and C are shown in black (darkest), green (lightest) and blue, respectively.

Highlights

- Struvite pre-precipitation essential for phosphate scaling control
- Multiple scale control strategies required for different precipitates
- Generalized precipitation models effective for the case of electrodialysis scaling